A tunable balanced phase shifter with wide operating bandwidth

Wei Zhang[1,2,3] , Binghe Wang[1], Bin Wang[1,4], Jin Shi[1,2,3] and Kai Xu[1,2,3]

[1]School of Information Science and Technology, Nantong University, Nantong, China; [2]Research Center for Intelligent Information Technology, Nantong University, Nantong, China; [3]Nantong Key Laboratory of Advanced Microwave Technology, Nantong University, Nantong, China and [4]R&D Department, Zhongtian Radio Frequency Cable Co., Ltd., Nantong, China

Abstract

A wideband tunable balanced phase shifter is achieved by utilizing varactor-loaded coupled lines (VLCLs)-embedded multistage branch-line structure. The tunable phase shift with low in-band phase deviation is attributed to the regulation in phase shift of the VLCLs and the horizontal microstrip lines in series. The wideband differential-mode (DM) impedance matching and common-mode (CM) suppression are due to multiple DM transmission poles and CM transmission zeros, which are brought about by the cascade of VLCLs and a microstrip line with short-circuited stubs in the DM-equivalent circuit and open-circuited stubs in the CM-equivalent circuit, respectively. Compared with the state-of-the-art tunable balanced phase shifters, the proposed design not only has the advantages of wide operating bandwidth (BW) with low in-band phase deviation but also has low insertion loss and easily fabricated structure. Theoretical analysis and design procedure were conducted, resulting in a prototype covering the frequency of 1.8 GHz. This prototype offers a tunable phase shift capability ranging from 0° to 90°. The prototype exhibits an operating BW of 45%, with a maximum phase deviation of $\pm 6°$. It also achieves a 10 dB DM return loss and CM suppression, while maintaining a maximum insertion loss of 2.5 dB.

Introduction

Tunable phase shifters play an important role in modern wireless communication systems such as phased arrays, beamforming networks, and antenna-feeding networks [1–3] due to their ability to provide continuous phase shifts. A wideband tunable phase shifter with low in-band phase deviation is becoming progressively appealing due to its ability to enhance data transmission rates and ensure optimal compatibility. Compared with the single-ended wideband tunable phase shifter, the balanced design has the additional advantages of easy connection with other balanced circuits and high immunity to electromagnetic interference. Therefore, the wideband tunable balanced phase shifter has become an essential component in modern communication systems. However, the CM suppression should be considered while designing the balanced phase shifters. Thus, wideband CM suppression covering the DM bandwidth (BW) is the primary challenge of the balanced designs. The other design challenges for a wideband tunable balanced phase shifter include wideband DM impedance matching, low in-band phase deviation, low insertion loss, and easy fabrication.

Various wideband tunable phase shifters have been reported, most of which are single-ended designs [4–15]. Some wideband tunable phase shifters are designed using a 3-dB coupler with different reflective loads [4–9] or an all-pass topology based on coupled lines and varactors [10]. However, the operating BWs of these designs are around or below 12%. In [11], the variable odd-mode impedance of parallel-coupled lines is employed to expand the operating BW to 22.2%. This approach can realize the 45° tunable phase shift with a phase deviation of $\pm 4.5°$. Reference [12] increases the operating BW to 36% and extends the tunable phase shift range to 360° with a phase deviation of $\pm 15°$ by adding a varactor and an inductor to the terminals of parallel-coupled lines in the design of [11]. In [13], a multimode resonator is used to achieve the 360° tunable phase shifter with a low phase deviation of just $\pm 5.5°$, while the operating BW is only 26.1%. To further enhance the operating BW, a power dividing circuit and two 3-dB hybrids terminated with different circuits are applied to achieve the operating BW of 40% in [14]. The design provides the 104° tunable phase shift range with a phase deviation of $\pm 8.6°$. The above discussion demonstrates that it is still difficult to achieve the wide operating BW, low in-band phase deviation, and large phase shift range simultaneously in designing the tunable phase shifter.

So far, a few balanced phase shifters have been reported [16–23]. The approaches utilized in these balanced phase shifters include coupled lines with loaded transmission lines [16–20],

asymmetric structure [21], T-shaped multimode resonators with intermediate cascaded stubs [22], and slotline-based quasi-Schiffman structure [23]. However, these balanced phase shifters [16–23] provide discrete phase shift values. To the best of the authors' knowledge, only one balanced tunable phase shifter exhibiting good common-mode (CM) suppression has been reported [24]. However, the multilayer substrates with defected ground led to a complex structure, and the in-band phase deviation is significant.

In this paper, the varactor-loaded coupled lines (VLCLs)-embedded multistage branch-line structure is used to design the wideband tunable balanced phase shifter. The proposed design simultaneously achieves the tunable differential-mode (DM) phase shift with low in-band phase deviation, wideband DM impedance matching, wideband CM suppression, low insertion loss, and an easily fabricated structure. Compared with the authors' previous design [18], 0°–90° tunable phase shift and the same circuit used by the reference and main lines for 0°–90° phase shifters make the proposed design more suitable for different scenarios. Theoretical analysis is carried out by the network analysis method. The detailed design procedure is summarized to guide the practical design. A prototype is designed and fabricated to verify the theoretical prediction.

Proposed tunable balanced phase shifter

Figure 1 illustrates the circuit model of the proposed tunable balanced phase shifter. It consists of three cascaded branch-line structures that are configured by two horizontal VLCLs (Z_{co}, Z_{ce}, θ_c, C_v) at each side, two horizontal microstrip lines (Z_5, θ_5) at the center, four vertical branches from left to right (Z_1, θ_1, Z_2, θ_2, Z_3, θ_3, Z_4, θ_4), two open-circuited stubs (Z_{s1}, θ_{s1}, Z_{s2}, θ_{s2}) attached to the middle of two of the vertical branches, and two differential ports (ports 1-2). Since the entire circuit is symmetric along the center symmetrical line, the odd- and even-mode analysis method can be utilized to predict the DM and CM responses.
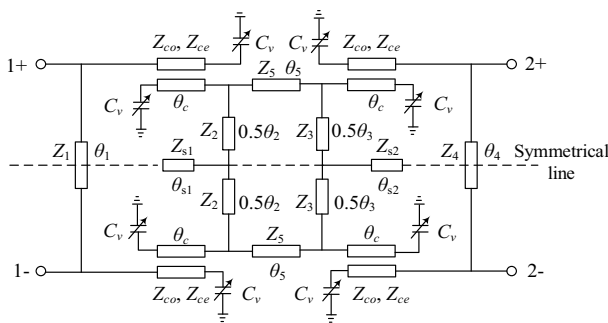

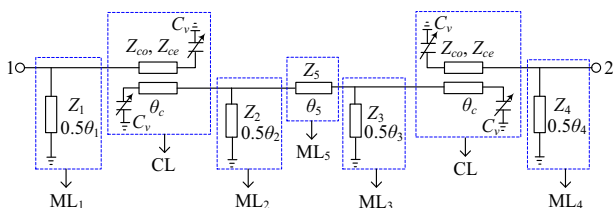**Figure 1.** Circuit model of the proposed tunable balanced phase shifter.

Figure 2. DM-equivalent circuit of the proposed tunable balanced phase shifter.

DM analysis

It can be seen from Fig. 1 that for the DM operation, a perfect electrical wall appears on the symmetrical plane. Thus, the DM-equivalent circuit can be obtained as shown in Fig. 2. To obtain the S-parameters of the DM-equivalent circuit, the ABCD matrix of Fig. 2 is required, which can be expressed as

$$\begin{bmatrix} A & B \\ C & D \end{bmatrix}^o = \begin{bmatrix} A & B \\ C & D \end{bmatrix}^o_{ML1} \begin{bmatrix} A & B \\ C & D \end{bmatrix}^o_{CL} \begin{bmatrix} A & B \\ C & D \end{bmatrix}^o_{ML2}$$
$$\begin{bmatrix} A & B \\ C & D \end{bmatrix}^o_{ML5} \begin{bmatrix} A & B \\ C & D \end{bmatrix}^o_{ML3} \begin{bmatrix} A & B \\ C & D \end{bmatrix}^o_{CL} \begin{bmatrix} A & B \\ C & D \end{bmatrix}^o_{ML4} \quad (1)$$

where

$$\begin{bmatrix} A & B \\ C & D \end{bmatrix}^o_{MLm} = \begin{bmatrix} 1 & 0 \\ -j\cot(0.5\theta_m)/Z_m & 1 \end{bmatrix} \quad (2)$$

where $m = 1, 2, 3$ or 4.

$$\begin{bmatrix} A & B \\ C & D \end{bmatrix}^o_{ML5} = \begin{bmatrix} \cos\theta_5 & jZ_5\sin\theta_5 \\ j\sin\theta_5/Z_5 & \cos\theta_5 \end{bmatrix} \quad (3)$$

$$\begin{bmatrix} A & B \\ C & D \end{bmatrix}^o_{CL} = \begin{bmatrix} Z_{11}/Z_{21} & (Z_{11}Z_{22} - Z_{12}Z_{21})/Z_{21} \\ 1/Z_{21} & Z_{22}/Z_{21} \end{bmatrix} \quad (4)$$

Z_{11}, Z_{12}, Z_{21}, and Z_{22} can be expressed as

$$Z_{11} = Z_{22} = Z_{c11} + \frac{(\omega^2 C_v^2 Z_{c11} - j\omega C_v)(Z_{c11}^2 + Z_{c14}^2) - 2\omega^2 C_v^2 Z_{c12} Z_{c13} Z_{c14}}{(1 + j\omega C_v Z_{c11})^2 + \omega^2 C_v^2 Z_{c13}^2} \quad (5)$$

$$Z_{21} = Z_{12} = Z_{c13} + \frac{2(\omega^2 C_v^2 Z_{c11} - j\omega C_v)Z_{c12} Z_{c14} - \omega^2 C_v^2 Z_{c13}(Z_{c12}^2 + Z_{c14}^2)}{(1 + j\omega C_v Z_{c11})^2 + \omega^2 C_v^2 Z_{c13}^2} \quad (6)$$

$$Z_{c11} = -j0.5(Z_{ce} + Z_{co})\cot\theta_c \quad (7)$$

$$Z_{c12} = -j0.5(Z_{ce} - Z_{co})\cot\theta_c \quad (8)$$

$$Z_{c13} = -j0.5(Z_{ce} - Z_{co})\csc\theta_c \quad (9)$$

$$Z_{c14} = -j0.5(Z_{ce} + Z_{co})\csc\theta_c \quad (10)$$

The DM phase shift can be written as

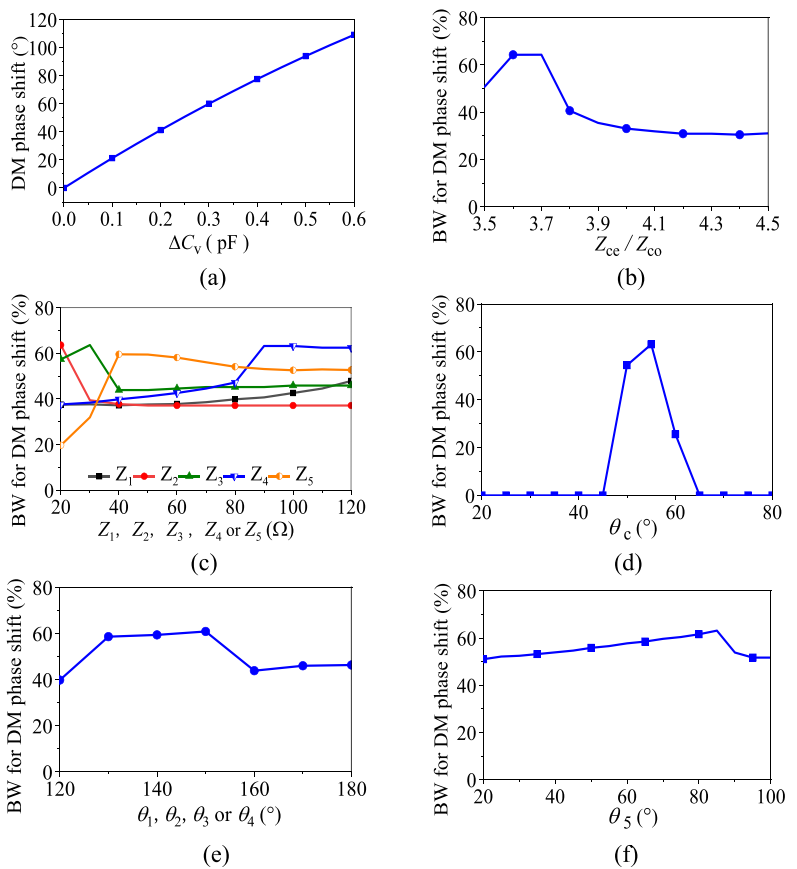$$\Delta\varphi = \angle S_{21}^{dd}(C_{v1}) - \angle S_{21}^{dd}(C_{v2}) \quad (11)$$

S_{ij}^{dd} and S_{ij}^{cc} are DM and CM S-parameters, i and j are the port numbers, and d and c denote DM and CM, respectively.
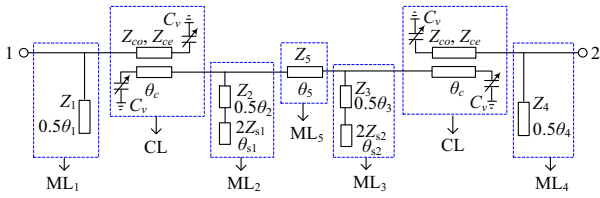
The BW for theoretical DM impedance matching can be calculated in MATLAB using Eqs. (1–10). Figure 3 exhibits the variations of the theoretical BW for 10-dB DM impedance matching with different C_v, Z_{ce}/Z_{co}, Z_1, Z_2, Z_3, Z_4, Z_5, θ_c, θ_1, θ_2, θ_3, θ_4, and θ_5. It can be seen from Fig. 3(a) that the BW for 10-dB DM impedance matching decreases with the increase in C_v. This is because the impedance of VLCLs changes with C_v, and the impedance matching deteriorates with an increase in C_v. Figure 3(b–f) depicts that the BW for 10-dB DM impedance matching increases at first and then decreases with the increase in Z_{ce}/Z_{co}, Z_2, Z_3, Z_5, θ_c, θ_1, θ_2, θ_3, θ_4 or θ_5. Conversely, the BW encounters an initial increase and then stabilizes when Z_1 or Z_4 is increased. Thus, a maximum BW
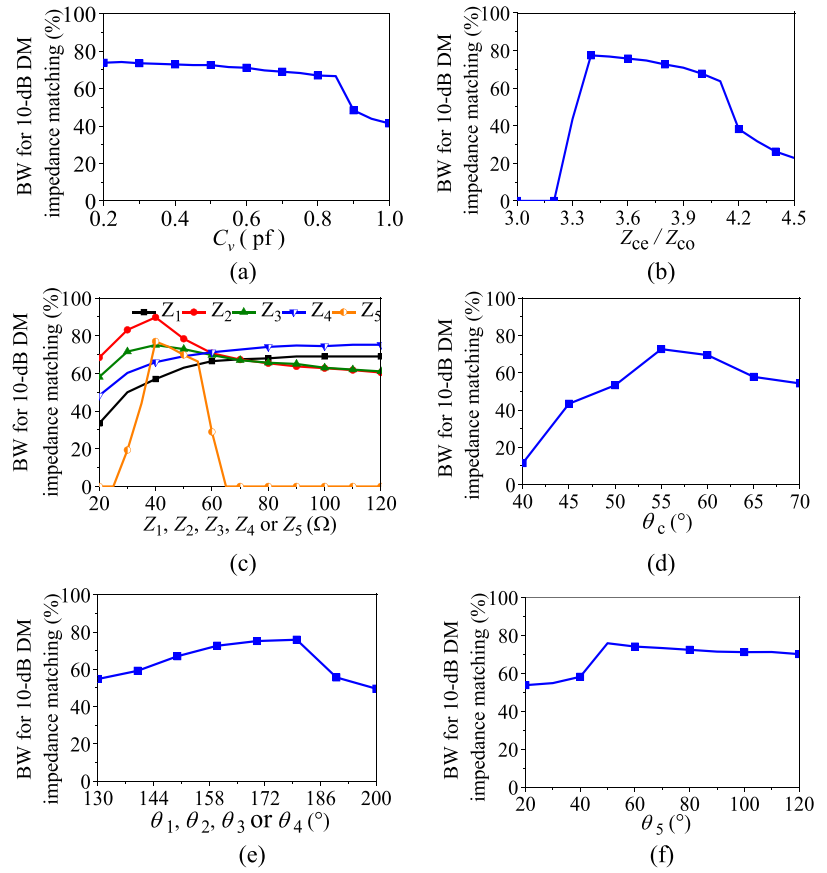
Figure 3. The calculated BW for 10-dB DM impedance matching varies with (a) C_v; (b) Z_{ce}/Z_{co}; (c) Z_1, Z_2, Z_3, Z_4, or Z_5; (d) θ_c; (e) θ_1, θ_2, θ_3, or θ_4; (f) θ_5 ($C_v = 0.3$ pF, $Z_{ce} = 150$ Ω, $Z_{co} = 40$ Ω, $Z_1 = 110$ Ω, $Z_2 = 22$ Ω, $Z_3 = 31$ Ω, $Z_4 = 70$ Ω, $Z_5 = 43$ Ω, $\theta_c = 53°$, $\theta_1 = \theta_2 = \theta_3 = \theta_4 = 80°$, and $\theta_5 = 70°$).

Figure 4. The calculated DM phase shift properties vary with different parameters. (a) DM phase shift varies with different ΔC_v, and the BW for DM phase shift varies with (b) Z_{ce}/Z_{co}; (c) Z_1, Z_2, Z_3, Z_4, or Z_5; (d) θ_c; (e) θ_1, θ_2, θ_3, or θ_4; (f) θ_5 ($C_v = 0.3$ pF, $Z_{ce} = 150$ Ω, $Z_{co} = 40$ Ω, $Z_1 = 110$ Ω, $Z_2 = 22$ Ω, $Z_3 = 31$ Ω, $Z_4 = 70$ Ω, $Z_5 = 43$ Ω, $\theta_c = 53°$, $\theta_1 = \theta_2 = \theta_3 = \theta_4 = 80°$, and $\theta_5 = 70°$).

Figure 5. CM-equivalent circuit of the proposed tunable balanced phase shifter.

for 10-dB DM impedance matching can be achieved by properly selecting the above parameters.

Similarly, the theoretical DM phase shift properties can be calculated using Eqs. (1–11). Figure 4(a) illustrates the variations of the theoretical DM phase shift with different ΔC_v ($\Delta C_v = C_{v2} - C_{v1}$, $C_{v1} = 0.3$pF). It can be observed from Fig. 4(a) that the DM phase shift increases with the increase in ΔC_v. This is because the electrical lengths of the VLCLs decrease when C_v is increased. Therefore, the tunable DM phase shift can be realized by varying the DC biasing voltage of the varactors.

Figure 4(b–f) exhibits the variations of the theoretical BW for DM phase shift with different Z_{ce}/Z_{co}, Z_1, Z_2, Z_3, Z_4, Z_5, θ_c, θ_1, θ_2, θ_3, θ_4, and θ_5 under the condition of the phase deviation within $\pm6°$. Here, if the phase deviation exceeds $\pm6°$ at the center frequency (f_0), the BW of the DM phase shift will be set as zero. It can be seen from Fig. 4(b–f) that the BW for DM phase shift initially expands, followed by a contraction with the increase in Z_{ce}/Z_{co}, Z_3, Z_4, Z_5, θ_c, θ_1, θ_2, θ_3, θ_4, or θ_5. Conversely, a marginal increase in BW is observed with a rise in Z_1, while a decrease followed by a nearly constant level occurs as Z_2 is increased. Furthermore, it can also be found from Fig. 4 that Z_{ce}/Z_{co}, Z_5, θ_c, and θ_5 have obvious effects on

the BW for DM phase shift. Thus, a maximum BW for DM phase shift can be obtained by properly selecting the parameters of the coupled lines and the microstrip lines in series.

CM analysis

For CM operation, the symmetric plane behaves as a perfect magnetic wall and the CM-equivalent circuit is depicted in Fig. 5. Similar to DM analysis, the theoretical CM performance can be obtained from the S-parameters of the CM-equivalent circuit, and the $ABCD$ matrix of Fig. 5 can be written as Eq. (12).

$$
\begin{bmatrix} A & B \\ C & D \end{bmatrix}^e = \begin{bmatrix} A & B \\ C & D \end{bmatrix}^e_{ML1} \begin{bmatrix} A & B \\ C & D \end{bmatrix}^e_{CL} \begin{bmatrix} A & B \\ C & D \end{bmatrix}^e_{ML2}
$$
$$
\begin{bmatrix} A & B \\ C & D \end{bmatrix}^e_{ML5} \begin{bmatrix} A & B \\ C & D \end{bmatrix}^e_{ML3} \begin{bmatrix} A & B \\ C & D \end{bmatrix}^e_{CL} \begin{bmatrix} A & B \\ C & D \end{bmatrix}^e_{ML4} \quad (12)
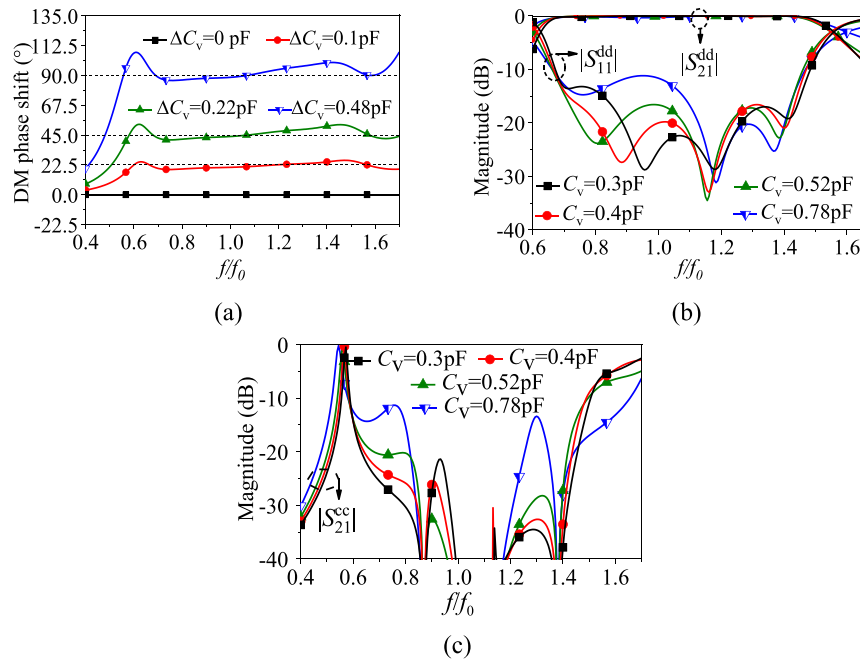$$

where the $ABCD$ matrices of the CL and ML_5 in Fig. 5 are equal to the $ABCD$ matrices of CL and ML_5 in Fig. 2, respectively, and

$$
\begin{bmatrix} A & B \\ C & D \end{bmatrix}^e_{MLn} = \begin{bmatrix} 1 & 0 \\ j\tan(0.5\theta_n)/Z_n & 1 \end{bmatrix} \quad (13)
$$

$$
\begin{bmatrix} A & B \\ C & D \end{bmatrix}^e_{ML2} =
$$
$$
\begin{bmatrix} \cos(0.5\theta_2) - \dfrac{Z_2 \sin(0.5\theta_2)\tan\theta_{s1}}{2Z_{s1}} & jZ_2\sin(0.5\theta_2) \\[2ex] \dfrac{j\sin(0.5\theta_2)}{Z_2} + \dfrac{j\cos(0.5\theta_2)\tan\theta_{s1}}{2Z_{s1}} & \cos(0.5\theta_2) \end{bmatrix} \quad (14)
$$
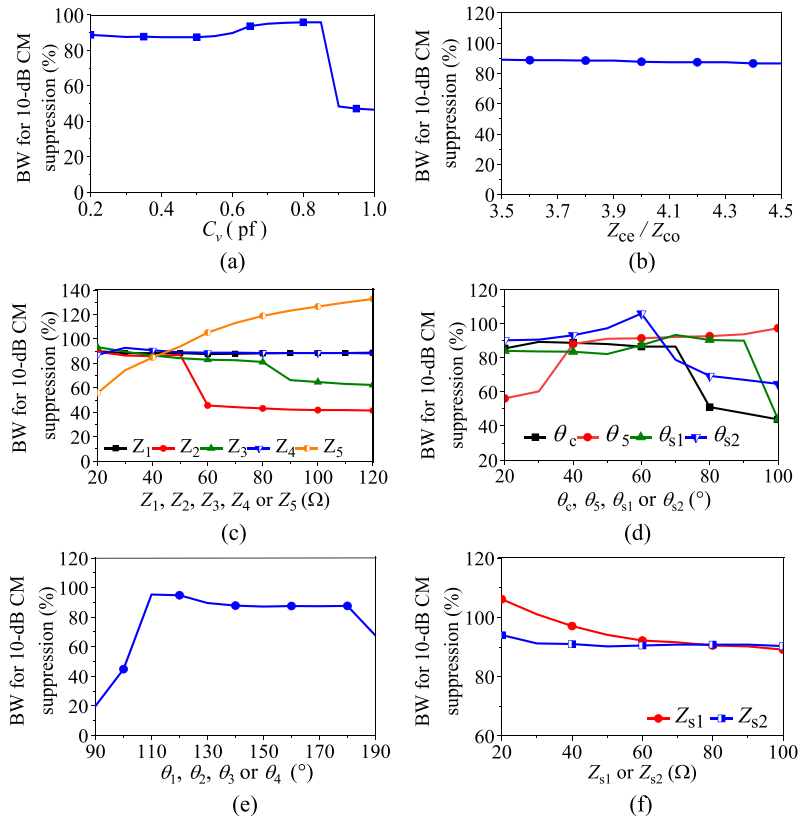
Figure 6. The calculated BW for 10-dB CM suppression varies with (a) C_v; (b) Z_{ce}/Z_{co}; (c) Z_1, Z_2, Z_3, Z_4, or Z_5; (d) θ_c, θ_5, θ_{s1}, or θ_{s2}; (e) θ_1, θ_2, θ_3, or θ_4; (f) Z_{s1} or Z_{s2} ($C_v = 0.3$ pF, $Z_{ce} = 150$ Ω, $Z_{co} = 40$ Ω, $Z_1 = 110$ Ω, $Z_2 = 22$ Ω, $Z_3 = 31$ Ω, $Z_4 = 70$ Ω, $Z_5 = 43$ Ω, $\theta_c = 53°$, $\theta_1 = \theta_2 = \theta_3 = \theta_4 = 80°$, $\theta_5 = 70°$, $Z_{s1} = 79$ Ω, $Z_{s2} = 60$ Ω, $\theta_{s1} = 80°$, and $\theta_{s2} = 30°$).

Figure 7. The theoretic responses of the case. (a) DM phase shift with different ΔC_v ($\Delta C_v = C_{v2}$- C_{v1}, $C_{v1} = 0.3$ pF). (b) DM S-parameters with different C_v. (c) CM S-parameters with different C_v.

$$
\begin{bmatrix} A & B \\ C & D \end{bmatrix}^e_{\text{ML3}} =
$$

$$
\begin{bmatrix} \cos(0.5\theta_3) - \dfrac{Z_3 \sin(0.5\theta_3)\tan\theta_{s2}}{2Z_{s2}} & jZ_3\sin(0.5\theta_3) \\[2ex] \dfrac{j\sin(0.5\theta_3)}{Z_3} + \dfrac{j\cos(0.5\theta_3)\tan\theta_{s2}}{2Z_{s2}} & \cos(0.5\theta_3) \end{bmatrix} \quad (15)
$$

The theoretical BW for CM suppression can be calculated from Eqs. (12–15). Figure 6 illustrates the theoretical BW for 10-dB CM suppression with different C_v, Z_{ce}/Z_{co}, Z_1, Z_2, Z_3, Z_4, Z_5, θ_1, θ_2, θ_3, θ_4, and θ_5. It can be noted from Fig. 6(a), (d), and (e) that the BW for 10-dB CM suppression initially increases followed by a decrease with the increase in C_v, θ_1, θ_2, θ_3, θ_4, θ_c, θ_{s1}, or θ_{s2}. Figure 6(b), (c), and (f) depict that the BW for 10-dB CM suppression remains almost unchanged with different Z_{ce}/Z_{co}, Z_1, Z_4, or Z_{s2}. However, it decreases with the increase in Z_2, Z_3, or Z_{s1}, while it increases when Z_5 or θ_5 is increased. Additionally, it can also be observed from Fig. 6 that Z_2, Z_3, Z_5, and θ_5 have significant impacts on the BW for CM suppression. Therefore, Z_2, Z_3, Z_5, and θ_5 can be used to obtain the wideband CM suppression.

According to Figs. 3, 4, and 6, it can be found that Z_{ce}/Z_{co}, Z_1, Z_4, and θ_c have significant effects on the DM performance but they do not impact the CM performance. Therefore, Z_{ce}/Z_{co}, Z_1, Z_4, and θ_c can be utilized to obtain the wideband DM performance. However, Z_{s1}, Z_{s2}, θ_{s1}, and θ_{s2} only affect the CM performance. Thus, Z_{s1}, Z_{s2}, θ_{s1}, and θ_{s2} can be used to improve the BW for CM suppression without affecting the DM performance. Moreover, the BWs for DM impedance matching and CM suppression are usually wider than those for DM phase shift. Thus, the operating BW is determined by the BW for the DM phase shift.

Design procedure

The theoretical design procedure is summarized as follows:
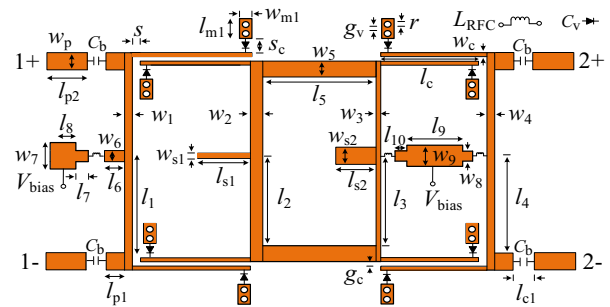
Figure 8. Layout of the proposed tunable balanced phase shifter.

(1) Choose varactors according to the required capacitance range.

(2) Determine Z_{ce}/Z_{co}, Z_1, Z_2, Z_3, Z_4, and Z_5 for the wide BWs of 10-dB DM impedance matching, DM phase shift, and 10-dB CM suppression in Fig. 3(b–c), Fig. 4(b–c), and Fig. 6(b–c), respectively.

(3) Determine θ_c, θ_1, θ_2, θ_3, θ_4, and θ_5 at f_0 for the wide BWs of 10-dB DM impedance matching, DM phase shift, and 10-dB CM suppression in Fig. 3(d–f), Fig. 4(d–f), and Fig. 6(d–e), respectively.

(4) Determine Z_{s1}, Z_{s2}, θ_{s1}, and θ_{s2} for the maximum BW of CM suppression according to the theoretical variations in Fig. 6(d) and (f).

Theoretic case

A design case with the tunable phase shift range of 0°–90° is demonstrated. According to Fig. 4, the BW for DM phase shift can achieve 60%. Thus, the operating BW is set as 60%, while the BWs for 10-dB DM impedance matching and 10-dB CM suppression can be set as large as possible, such as 80% and 90%, respectively.

Table 1. Dimensions of the proposed design (unit: mm)

w_c	g_c	l_c	w_1	l_1	w_2	l_2	w_3	l_3	w_4	l_4	w_5
0.3	0.12	19.67	0.25	21.15	1.25	19.39	0.54	19.39	1.01	21.15	2.11
l_5	w_{s1}	l_{s1}	w_{s2}	l_{s2}	s	s_c	w_{m1}	l_{m1}	r	g_v	w_6
20.5	0.53	7.25	5	7.1	0.5	0.6	0.8	1.5	0.2	0.2	2
l_6	w_7	l_7	w_8	l_8	w_9	l_9	l_{10}	l_{p1}	l_{c1}	l_{p2}	w_p
1	5	1.5	2	3	5	15.17	1.5	1.8	1	8	1.83
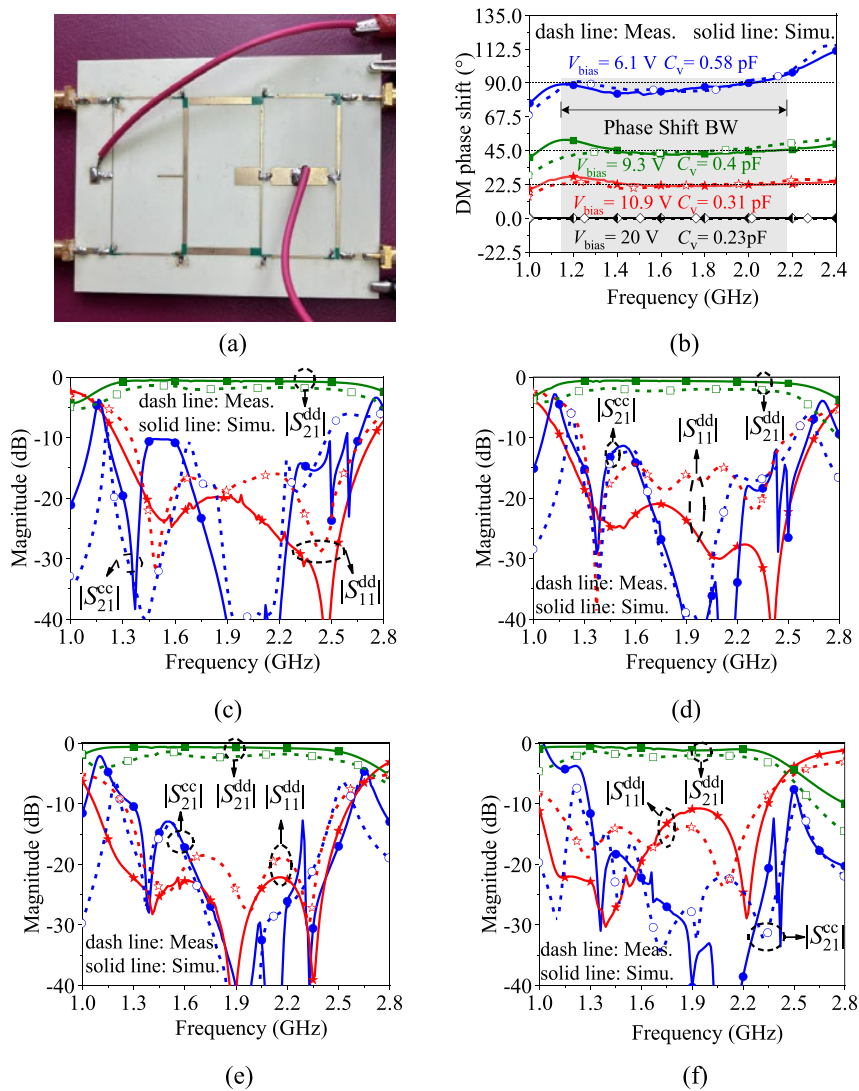
Figure 9. The photograph, simulated (Simu.), and measured (Meas.) results of the proposed design. (a) Photograph. (b) DM phase shift with different C_v and different V_{bias}. (c) S-parameters for $C_v = 0.23$ pF and $V_{bias} = 20$ V. (d) S-parameters for $C_v = 0.31$ pF and $V_{bias} = 10.9$ V. (e) S-parameters for $C_v = 0.4$ pF and $V_{bias} = 9.3$ V. (f) S-parameters for $C_v = 0.58$ pF and $V_{bias} = 6.1$ V.

According to the design procedure and the targets, the theoretic parameters (C_v, Z_{ce}/Z_{co}, Z_1, Z_2, Z_3, Z_4, Z_5, Z_{s1}, Z_{s2}, θ_c, θ_1, θ_2, θ_3, θ_4, θ_5, θ_{s1}, and θ_{s2}) can be obtained as follows: $Z_{ce} = 143\ \Omega$, $Z_{co} = 38\ \Omega$, $\theta_c = 53°$, $Z_1 = 110\ \Omega$, $Z_2 = 22\ \Omega$, $Z_3 = 31\ \Omega$, $Z_4 = 70\ \Omega$, $\theta_1 = \theta_2 = \theta_3 = \theta_4 = 80°$, $Z_5 = 43\ \Omega$, $\theta_5 = 70°$, $Z_{s1} = 79\ \Omega$, $\theta_{s1} = 80°$, $Z_{s2} = 60\ \Omega$, $\theta_{s2} = 30°$, $C_{v,\,0°} = 0.3$ pF, $C_{v,\,22.5°} = 0.4$ pF, $C_{v,\,45°} = 0.52$ pF, $C_{v,\,90°} = 0.78$ pF. Then the theoretic responses of the case can be obtained by using the microwave network theory, as shown in Fig. 7. It can be observed from Fig. 7 that the theoretic responses agree well with the target performances.

Implementation and results

A prototype working at 1.8 GHz with the tunable phase shift range of 90° is designed, fabricated, and measured to validate the proposed method. Figure 8 exhibits the layout of the proposed design, which is a single-layer substrate circuit and is designed on the substrate of Ro4003C (the dielectric constant of 3.38, loss tangent of 0.0027, and $h = 0.813$ mm). The software for full-wave simulation is Ansoft High Frequency Structure Simulated.

Table 2. Performance comparison with previous works

	f_0 (GHz)	$\Delta\varphi_{max}$ (°)	$\Delta\varphi_{max\_err}$ (°)	IL_{max} (dB)	RL_{min} (dB)	BW_{IM} (%)	BW_{PS} (%)	BW_{CMS} (%)	FoM (°/dB)	T	Type
[5]	2.15	121	N/A	0.72	15	15	N/A	N/A	169	Y	Single-end
[6]	2	234	±16	4.6	12	10	10	N/A	50.9	Y	Single-end
[7]	2	390	±20	4.2	14	10	10	N/A	92.9	Y	Single-end
[8]	2	385	±15	1	10.9	10	10	N/A	385	Y	Single-end
[9]	10	190	±10	2	10	10	10	N/A	95	Y	Single-end
[10]	7.2	380	±11	4.2	9.4	13.9	13.9	N/A	90.5	Y	Single-end
[11]	2.25	45	±4.5	1.4	6	22	22	N/A	32.1	Y	Single-end
[12]	2.2	360	±15	3.2	10	36	36	N/A	112.5	Y	Single-end
[13]	1.72	360	±5.5	3.6	10.5	26.1	26.1	N/A	100	Y	Single-end
[14]	2.5	104	±8.6	1.06	16.5	40	40	N/A	98.1	Y	Single-end
[15]	2.5	147	±5.79	1.28	15.76	20	20	N/A	114.8	Y	Single-end
[16]	1	90	±5.5	0.74	15	80	93	77	N/A	N	Balanced
[17]	2	90	±4.8	1.27	13.7	56.6	59.5	275	N/A	N	Balanced
[18]	3.5	90	±4.7	0.78	15	83	81	86	N/A	N	Balanced
[21]	1.8	90	±3.7	2.4	14.7	53	53	150	N/A	N	Balanced
[22]	4	180	±4	0.9	15	67.5	68.5	92.5	N/A	N	Balanced
[23]	2.5	180	±4	0.79	10	59	54	100	N/A	N	Balanced
[24]	5.2	195	N/A	3.3	N/A	N/A	N/A	75	59	Y	Balanced
This work	1.8	90	±6	2.36	10	80	57.8	67.8	38.1	Y	Balanced

IL: insertion loss; RL: return loss; BW$_{IM}$: bandwidth for impedance matching; BW$_{PS}$: bandwidth for phase shift; BW$_{CMS}$: bandwidth for CM suppression; T: tunable; Y: Yes; N: No.

The initial dimensions of the proposed prototype are obtained according to the theoretic parameters given in the section "Theoretic case", and the final dimensions are given in Table 1. Additionally, C_b = 430 pF, L_{RFC} = 270 nH. SMV2201-040LF varactor (0.23–2.1 pF, 0–20 V) is utilized according to the capacitance range required in Fig. 7. Figure 9(a) shows the photograph of the proposed design, which was measured by a four-port Agilent N5230C vector network analyzer.

Figure 9(b–f) illustrates the simulated and measured results of the proposed design with different values of capacitance of varactors (C_v) and DC biasing voltages (V_{bias}). During the tuning, C_v increases from 0.23 to 0.58 pF corresponding to the decrease in V_{bias} from 20 V to around 6.1 V. Hence, a tunable balanced 0°–90° phase shifter is achieved. The measured BW for 0°–90° DM phase shift with a maximum phase deviation of ±6° spans from 1.13 to 2.17 GHz (57.8%). The measured BW for attaining a 10-dB DM return loss, considering different V_{bias}, spans from 1.35 to 2.31 GHz (53.3%), exhibiting a minimum DM insertion loss of 1.37 dB. Moreover, the measured BW for achieving 10-dB CM suppression across different V_{bias} values covers the range from 1.25 to 2.47 GHz (67.8%). The figure of merit (FoM) [8] of this design is 38.1°/dB. Thus, the operating BW is 1.35–2.17 GHz (45.5%), which is the frequency range simultaneously covering the 10-dB DM impedance matching, 10-dB CM suppression, and the phase deviation within ±6°. The RMS phase errors and RMS amplitude imbalance [25] in the operating BW are less than 2.98° and 1.58 dB, respectively. The measured results align with the simulated results. The measured insertion losses are slightly higher than the simulated ones, which may be due to parasitic components of the varactors and inconsistencies in the implementation.

The performances of the proposed design and the state-of-the-art designs are listed in Table 2. It can be seen from the table that compared with the single-ended tunable phase shifters in [5–15], the proposed design has the function of CM suppression in addition to DM tunable phase shift. Moreover, the proposed design can provide DM tunable phase shifts compared with the balanced designs with discrete phase shifts in [16–18] and [21–23]. Furthermore, compared with the tunable balanced phase shifter in [24], the proposed one is a single-layer design with an easier-fabricated structure and also has the advantages of lower in-band phase deviation, wider BW for DM impedance matching, and lower insertion loss.

Conclusion

In this paper, a wideband tunable balanced phase shifter using the VLCLs-embedded multistage branch-line structure is proposed. Complete theoretical analysis and design procedure are presented to guide the practical design. A prototype with a tunable phase shift range of 90° is designed and measured. Experimental results and comparative analysis validate that compared with the state-of-the-art tunable balanced phase shifter, the proposed design simultaneously presents advantages such as a wideband flat phase shift, wideband DM impedance matching, wideband CM suppression, low insertion loss, and an easily fabricated structure. Benefiting from these features, it is believed that the proposed tunable balanced phase shifter holds the potential to promote the development of modern wireless communication systems.

References

1. **Sazegar M, Zheng Y, Maune H, Damm C, Zhou X and Jakoby R** (2011) Compact tunable phase shifters on screen-printed BST for balanced phased arrays. *IEEE Transaction on Microwave Theory and Techniques* **59**, 3331–3337.
2. **Ren H, Li P, Gu Y and Arigong B** (2020) Phase shifter-relaxed and control-relaxed continuous steering multiple beamforming 4 × 4 butler matrix phased array. *IEEE Transactions on Circuits and Systems I: Regular Papers* **67**, 5031–5038.
3. **Hu J, Yang X, Ge L and Wong H** (2022) A polarization and beam steering reconfigurable cavity-backed magneto-electric dipole antenna array using reflection-type phase shifter. *IEEE Transactions on Antennas and Propagation* **70**, 296–306.
4. **Han SM, Kim CS, Ahn D and Itoh T** (2005) Phase shifter with high phase shifts using defected ground structures. *Electronics Letters* **41**, 196–197.
5. **Occello O, Tiague L, Margalef-Rovira M, Vincent L, Ndagijimana F and Ferrari P** (2021) High-performance compact reflection-type phase shifter operating at 2 GHz using a transdirectional coupler. In *Proceedings of the 50th European Microwave Conference*, 1–4.
6. **Lin C-S, Chang S-F, Chang -C-C and Shu Y-H** (2007) Design of a reflection-type phase shifter with wide relative phase shift and constant insertion loss. *IEEE Transactions on Microwave Theory and Techniques* **55**, 1862–1868.
7. **Lin C-S, Chang S-F and Hsiao W-C** (2008) A full-360° reflection-type phase shifter with constant insertion loss. *IEEE Microwave and Wireless Components Letters* **18**, 106–108.
8. **Burdin F, Iskandar Z, Podevin F and Ferrari P** (2015) Design of compact reflection-type phase shifters with high figure-of-merit. *IEEE Transactions on Microwave Theory and Techniques* **63**, 1883–1893.
9. **Singh A and Mandal MK** (2020) Electronically tunable reflection type phase shifters. *IEEE Transactions on Circuits and Systems II: Express Briefs* **67**, 425–429.
10. **Khoder K, Roy ML and Pérennec A** (2014) An all-pass topology to design a 0-360° continuous phase shifter with low insertion loss and constant differential phase shift. In *Proceedings of the 44th European Microwave Conference*, 1–4.
11. **Abbosh AM** (2012) Tunable phase shifter employing variable odd-mode impedance of short-section parallel-coupled microstrip lines. *IET Microwaves, Antennas & Propagation* **6**, 305–311.
12. **Abbosh AM** (2012) Compact tunable reflection phase shifters using short section of coupled lines. *IEEE Transactions on Microwave Theory and Techniques* **60**, 2465–2472.
13. **Li H, Guo X, Yu T, Zhu L and Wu W** (2022) Wideband continuously tunable phase shifter with phase slope tunability and low phase error. *IEEE Transactions on Microwave Theory and Techniques* **70**, 2147–2155.
14. **Chaudhary G and Jeong Y** (2019) Wideband tunable differential phase shifter with minimized in-band phase deviation error. *IEEE Microwave and Wireless Components Letters* **29**, 468–470.
15. **An B, Chaudhary G and Jeong Y** (2018) Wideband tunable phase shifter with low in-band phase deviation using coupled line. *IEEE Microwave and Wireless Components Letters* **28**, 678–680.
16. **Zhang W and Shi J** (2019) A balanced phase shifter with common-mode suppression. *IEEE Transactions on Industrial Electronics* **66**, 378–386.
17. **Qiu -L-L and Zhu L** (2019) Balanced wideband phase shifters with good filtering property and common-mode suppression. *IEEE Transactions on Microwave Theory and Techniques* **67**, 2313–2321.
18. **Zhang W, Xu K, Shi J and Shen Z** (2020) A compact single-layer balanced phase shifter with wide bandwidth and uniform reference line. *IEEE Access* **8**, 41530–41536.
19. **Alizadeh MK, Shamsi H, Tavakoli MB and Aliakbarian H** (2020) Simple ladder-like single-layer balanced wideband phase shifter with wide phase shift range and appropriate common-mode suppression. *IET Microwaves, Antennas & Propagation* **14**, 1137–1147.
20. **Shi J, Nie Y, Zhang W and Wu Y** (2021) Differential filtering phase shifter with wide common-mode suppression bandwidth and high frequency selectivity. *IEEE Transactions on Circuits and Systems II: Express Briefs* **68**, 2379–2383.
21. **Nie Y, Zhang W and Shi J** (2019) A compact balanced phase shifter with wideband common-mode suppression. *IEEE Access* **7**, 153810–153818.
22. **Qiu -L-L, Zhu L and Lyu Y-P** (2019) Balanced wideband phase shifters with wide phase shift range and good common-mode suppression. *IEEE Transactions on Microwave Theory and Techniques* **67**, 3403–3413.
23. **Han Y, Li R, Qiao L and Feng W** (2022) Balanced wideband quasi-schiffman phase shifters based on slotlines. *IEEE Transactions on Circuits and Systems II: Express Briefs* **69**, 4283–4287.
24. **Ding C, Meng F-Y, Jin T, Lv J-F, Mu H-L and Wu Q** (2020) Tunable balanced liquid crystal phase shifter based on spoof surface plasmon polaritons with common-mode suppression. *Liquid Crystals* **47**, 1612–1623.
25. **Zaiden DM, Grandfield JE, Weller TM and Mumcu G** (2018) Compact and wideband MMIC phase shifters using tunable active inductor-loaded. *IEEE Transactions on Microwave Theory and Techniques* **66**, 1047–1057.

Wei Zhang received the B.S. degree in integrated circuit design and integrated system from Nantong University, Nantong, China, in 2008, the M.S. and Ph.D. degrees in information and communication engineering from the Nantong University, Nantong, China, in 2011, and 2021, respectively. From 2011 to 2020, she was a lecturer at Xinglin College, Nantong University. In 2021, she joined the Research Center for Intelligent Information Technology, Nantong University, Nantong, China, as an Associate Professor. Her current research interests include RF/microwave components and circuits.

Binghe Wang was born in Quanzhou, Fujian, Province, China, in 1999. He received the B.S. degree in software engineering in 2022 from Guangxi Science & Technology Normal University, Laibin, China, where he is currently working toward the M.S. degree in electromagnetic field and microwave technology. His current research interests include RF/microwave components and antenna technology.

Bin Wang was born in 1984, in JiangSu Province, China. He graduated from Huazhong University of Science and Technology in 2008 and received a Bachelor's Degree in Electronic information and Engineering. He has engaged in wireless communication and leaky coaxial cable. He is the engineer of Technology Department of Zhongtian Radio Frequency Co., Ltd.

Jin Shi received the B.S. degree in physics education from HuaiYin Teachers College, Huai'an City, China, in 2001, the M.S. degree in radio physics from the University of Electronic Science and Technology of China, Chengdu, China, in 2004, and the Ph.D. degree in electronic engineering from the City University of Hong Kong, Hong Kong, in 2011. From 2007 to 2008, he was a Research Assistant with the City University of Hong Kong. He was a Research Fellow Institute for Infocomm Research, Singapore, where he was a scientist from 2011 to 2013. In 2013, he joined the School of Electronics and Information, Nantong University, China, as a Professor. From 2019, he was also a Group Leader of Research Center for Intelligent Information Technology. His current research interests include RF/microwave components and subsystems, antennas, differential circuit, and dielectric circuits and antennas.

Kai Xu was born in Haian, Jiangsu Province, China, in 1991. He received the B.Sc. degree from Taizhou Institute of Science and Technology, Jiangsu Province, China, in 2013, the M.S. degree from the Nantong University, Nantong, Jiangsu Province, China, in 2016, the Ph.D. degree from the Nantong University, Nantong, Jiangsu Province, China, in 2019, respectively. From 2015 to 2016, he was a Research Assistant of the Institute for Infocomm Research, Singapore. In 2020, he joined the Research Center for Intelligent Information Technology, Nantong University, China, as a Lecturer. His current research interests include microwave components, balanced microwave circuits, antennas, and integrated designs. He has served as a Reviewer for the *IEEE Transactions on Industrial Electronics, IEEE Microwave and Wireless Components Letters, IEEE Access and IET Electronic Letters*, and other publications.